Nuclear Materials and Energy 39 (2024) 101677

Contents lists available at ScienceDirect

Nuclear Materials and Energy

journal homepage: www.elsevier.com/locate/nme

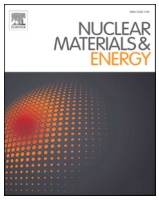

Laser-induced breakdown spectroscopy for helium detection in beryllium coatings

Indrek Jõgi [a,*], Peeter Paris [a], Jasper Ristkok [a], Alicia Marin Roldán [b], Pavitra Ganapati Bhat [b], Pavel Veis [b], Juuso Karhunen [c], Salvatore Almaviva [d], Wojciech Gromelski [e], Paul Dinca [f], Corneliu Porosnicu [f], Iva Bogdanović Radović [g], Zdravko Siketić [g], Paweł Gąsior [e], Jari Likonen [c], Antti Hakola [c]

[a] Institute of Physics, University of Tartu, W. Ostwaldi str. 1, 50411 Tartu, Estonia
[b] DEP, FMPI, Comenius University, Mlynská dolina F2, 842 48 Bratislava, Slovakia
[c] VTT, P. O. Box 1000, 02044 VTT, Finland
[d] ENEA, Italian National Agency for New Technologies, Energy and Sustainable Economic Development, Frascati Research Center, via Enrico Fermi, 45, I-00044 Frascati, Italy
[e] IPPLM Institute of Plasma Physics and Laser Microfusion, Hery Street 23, 01-497 Warsaw, Poland
[f] INFLPR 409, Magurele, Jud Ilfov 077125, Bucharest, Romania
[g] Rudjer Boskovic Institute, PO Box 180, 10002 Zagreb, Croatia

ARTICLE INFO

Keywords:
LIBS
He retention
Be coatings

ABSTRACT

Laser Induced Breakdown Spectroscopy (LIBS) method is considered to be a promising tool for analyzing the retention of hydrogen isotopes (D and T) and helium (He) on the first walls and divertor regions of future fusion reactors. Helium will be produced in DT reactions but could also be used in the initial non-nuclear phases of DEMO concepts. The present study investigates the He detection by LIBS method in the Be coatings simulating the deposits on the divertor plasma-facing components of JET while the results are also relevant for He detection in the deposits of other wall materials. The study was carried out in a vacuum vessel filled with 2–40 mbar argon background gas. It was shown that 2.8 at. % of He was confidently detectable by LIBS at optimized measurement conditions and the estimated limit of detection at used experimental conditions is approximately 0.7 at. %. The intensity of the He emission line at 587.56 nm was the strongest at the center of the laser-induced plasma plume. The He line intensity increased with the pressure of Ar gas but the broadening of the He line and the increase of the background emission and noise set an upper limit to the Ar background pressure usable for He detection. The application of the calibration-free LIBS procedure resulted in the overestimation of the He/Be ratio by several orders of magnitude. The overestimation can be explained by the deviation of LIBS plasma from the local thermodynamic equilibrium, which is caused by the very high excitation energy of He atoms.

1. Introduction

Beryllium (Be) is used as the first wall material of the main chamber of Joint European Torus (JET) [1–3] because of its low atomic number, which allows the reduction of the adverse effects of the plasma contamination by erosion, its usefulness as a getter for oxygen and its reasonably good thermal and mechanical properties [1,4,5]. One of the issues investigated in JET is the hydrogen isotope (tritium (T) and deuterium (D)) retention in the plasma-facing components (PFCs) [1,3]. While Be has lower tritium retention when compared to carbon [1,6], the retention is still relatively high, mainly due to the co-deposition of hydrogen isotopes and Be on the divertor PFCs [6–9]. Besides the hydrogen isotopes used as fuel, helium (He) ash is inherently produced in fusion reactors and He retention in the co-deposits may influence the fuel retention [10,11]. Therefore, the detection of He in layers with variable composition and mechanical properties is an important research question that has relevance for the operation of International Thermonuclear Experimental Reactor (ITER) regardless of its main wall material.

There is a need for in-situ methods that can determine the retention

* Corresponding author.
E-mail address: indrek.jogi@ut.ee (I. Jõgi).

https://doi.org/10.1016/j.nme.2024.101677
Received 28 February 2024; Received in revised form 23 April 2024; Accepted 16 May 2024
Available online 18 May 2024

of fuel and other impurities in the ITER plasma-facing components. Laser-induced breakdown spectroscopy (LIBS) is one method considered for this purpose [12–16]. LIBS method uses a short (<100 ns) but intense laser pulse to melt, evaporate and ionize a small amount of the investigated material. The optical emission spectrum of the formed plasma plume is characteristic of the investigated material and can be used to determine the qualitative composition of the material. Quantitative composition can be determined after proper calibration of the LIBS spectra or by using calibration-free (CF) LIBS when certain experimental conditions are met. LIBS has been successfully used for D detection in Be containing coatings and the quantitative concentration of D determined by CF-LIBS is consistent with the D concentration determined by other methods [17–21].

The excitation energies of stronger He lines are approximately 23 eV, considerably higher than the excitation energy of 12 eV of the strongest D_α line at 656.1 nm. This large energy difference expectedly requires higher plasma plume temperatures for He detection. There have been only a few LIBS studies concerning He detection in tungsten (W) [22–25] and aluminum (Al) [26] and no studies concerning He detection in Be containing coatings. Therefore, the aim of the current study was to evaluate the usability of LIBS for He detection in Be coatings and explore optimal experimental parameters for He detection. Be coatings are used as proxies for co-deposits seen at JET and can represent other co-deposits in future reactors, such as B-O-W when B is used as a getter for oxygen instead of Be.

2. Experimental setup and methods

The samples simulating Be co-deposits with D and He were produced at the National Institute for Laser, Plasma and Radiation Physics in Romania by High Power Impulse Magnetron Sputtering (HiPIMS). The coating with a nominal thickness of 5 μm and a composition (in at. %): 5 % D, 5 % He and 90 % Be were prepared on W substrates. The measured thickness and composition values are given in the results section (Chapter 3.1). Mirror-polishing of high-purity (99.5 %) polycrystalline W was performed to replicate the pristine surface of the divertor and the chemical cleaning process was used to eliminate processing and organic residues [27]. The cleaned and polished substrates were affixed to the sample holder 10 cm away from the water-cooled magnetron plasma source which had a high-purity (99.95 %) Be metallic target. The source was driven by a HiPIMS generator connected to a high-voltage DC power supply (1 kV, 1 A) [27–29]. The reaction chamber was pumped down to a base pressure of 10^{-4} Pa and a glow discharge was initiated for 30 min in argon (Ar) background gas at pressure 4 Pa to clean the substrates from impurities. Subsequently, a cathodic discharge was initiated to remove impurities and surface oxides from the surface of Be target and to ensure good adhesion between the formed coating and the substrate. The deposition of He and D containing layer was made in He and D_2 flow (2 sccm and 40 sccm respectively) while the Ar process gas flow was (4 sccm) and total pressure was 2 Pa. The deposition process with a single plasma source took approximately 12 h to keep the substrate temperature below 60 °C which is well below the desorption threshold of He and D from the deposited layers. The deposition rate was determined by a quartz micro-balance and using extrapolations from previous experiments.

The composition of the formed Be coating was analyzed by Time-of-flight Elastic Recoil Detection Analysis (TOF-ERDA) and Secondary Ion Mass Spectroscopy (SIMS). TOF-ERDA measurements were done using 20 MeV $^{127}I^{6+}$ beam obtained from the Tandem VdG accelerator at the Ruđer Bošković Institute, Zagreb, Croatia. The angle between the sample surface and the incident ion beam was 20°. The spectrometer was placed at 37.5° toward the incident beam direction. More details about the experimental setup can be found in [30,31]. Analysis of TOF-ERDA spectra was done using the program Potku [32]. SIMS measurements were made by a double focusing magnetic sector SIMS (VG Ionex IX-70S). A 5 keV O_2^+ primary ion beam was applied, and the intensities of selected positive secondary ions were profiled as functions of time. The current of the primary ions was adjusted to 500 nA during the profiling, and the beam was raster-scanned across an area of 300 × 430 μm^2. A 10 % electronic gate and a 1 mm optical gate were used in all the measurements to eliminate the disturbing ejection of particles from the edges of the SIMS crater [33].

LIBS measurements were carried out in a vacuum system dedicated to LIBS measurements of Be-containing samples [18]. The schematic description of the experimental setup is shown in Fig. 1. Most of the measurements were carried out in an Ar atmosphere at 2 mbar while a series of measurements were made at pressures up to 40 mbar. The Quantum Brilliant B impulse Nd:YAG laser with 1064 nm wavelength and 5 ns pulse width was focused on the sample surface by a lens with a focal length of 500 mm. The energy of the laser pulse was 51 mJ and the corresponding fluence was 4–4.6 J/cm^2. The emission of the formed laser plasma plume was collected perpendicularly to the laser beam. The position along the plasma plume, where the emission was collected, could be varied. The emission was directed by an off-axis parabolic mirror onto the optical fibre bundle which guided the emission to the spectrometer. The movement of the mirror allowed to change the region of the plasma plume where the spectrum was collected and record the intensity of the lines as the function of the distance from the sample surface. The spectrometer was an Andor SR-750 coupled with an ICCD camera Andor iStar 340 T. The spectrometer grating with 600 grooves/mm with a blaze wavelength of 500 nm allowed to register the spectra in the spectral window of 40 nm with the resolution of 0.15 nm (Apparatus function of the spectrometer determined on the basis of FWHM of He-Ne laser line at 632.8 nm). The delay time between the laser pulse and the recording of the spectrum was 200 ns and the recording gate was also 200 ns. This delay time value was chosen because our unpublished studies with W coatings showed that at similar pressures and optical configuration, the highest signal-to-noise ratio for He 587.56 nm line intensity was obtained in the delay time range of 100–300 ns.

3. Results and discussion

3.1. ToF-ERDA and SIMS measurements

According to the TOF-ERDA measurements, the coatings contained 2.8 at. % He, 3.7 at. % D and 89 at. % Be (Fig. 2a) in the surface regions while there were also other impurities such as H, C, N, and O with concentrations up to 1 at. % (not shown). The H and O concentrations were higher at the surface of the coating while Be, D and He concentrations remained nearly constant throughout the depth accessible by ToF-ERDA (300–400 nm). The depth profiles determined by SIMS measurements show that the distribution of H and D was uniform through the coating with a somewhat higher H signal on the surface consistently with ToF-ERDA measurement (Fig. 2b). The signal from W substrate started to appear at about 4000 nm which suggests that the

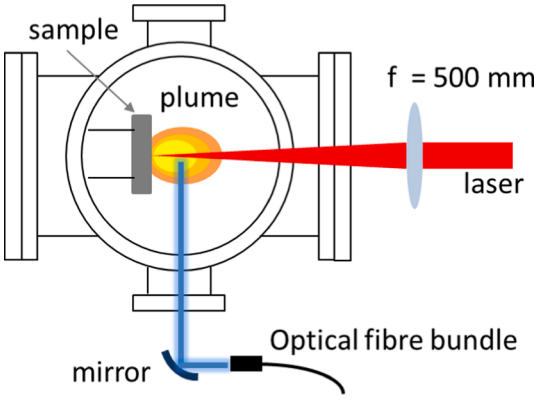

Fig. 1. Schematic of the experimental setup.

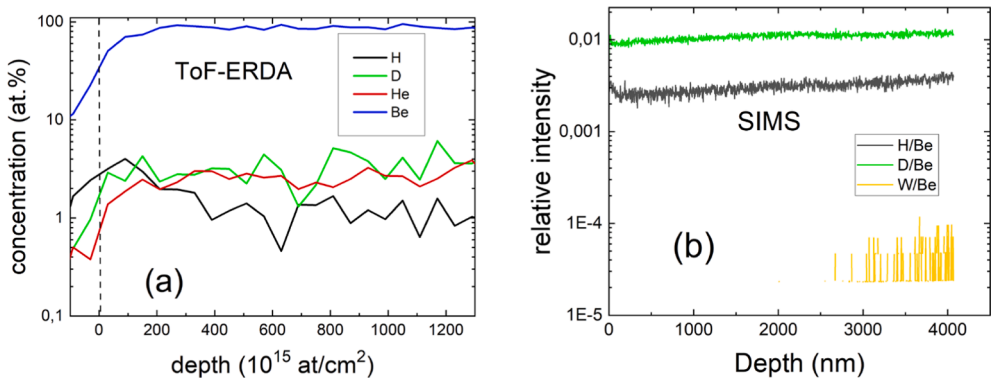

Fig. 2. (a) ToF-ERDA depth profiles of H, D, He and Be concentration in the first 100 nm of the Be coating and (b) SIMS depth profiles of H/Be, D/Be and W/Be ratios throughout the Be coating.

thickness of the coating was 4500–5000 nm and comparable with the nominal coating thickness of 5000 nm.

3.2. Determination of spectral line intensities

Exemplary spectra in the wavelength range of 372–413 nm collected for the 2nd and 100th laser shots at the same spot on the coating are shown in Fig. 3. During the first laser shots, the spectra were dominated by numerous Ar II lines and there was also a strong Be I 381.34 nm line. At 16th laser shot, W lines started to appear and Be I and Ar II lines started to decrease (see Fig. 5). At the 100th shot, the Be I line diminished to the noise level and Ar II lines became considerably weak, compared to the situation during the first laser shots. Similar trends for Be, Ar and W lines were observed in other wavelength ranges.

A reasonably strong and interference-free He line was observed at 587.56 nm (Fig. 4), when the spectra were collected from the central plasma plume region. At this relatively short delay time, the electron densities in the plasma plume were sufficiently large to cause considerable Stark broadening of He and Be lines. Therefore, the lines were fitted with Voigt profiles [34], with the variable width of the Lorentzian profile determined by the Stark broadening and the fixed width of the Gaussian profile defined by the apparatus function with the FWHM value of 0.15 nm. The W lines were fitted with Gaussian profiles. It should be noted that other relatively strong He lines at 388.86 nm, 447.15 nm and 667.82 nm were not detectable in the registered LIBS spectra or interfered with much stronger background lines arising mostly from Ar II.

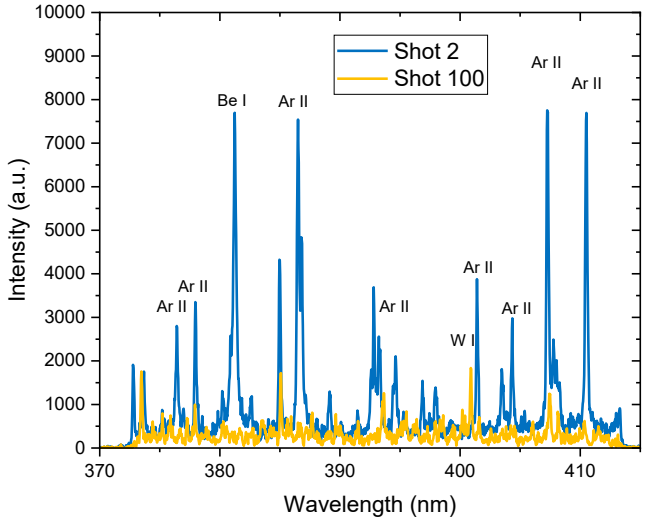

Fig. 3. LIBS spectra of laser shot 2 and 100 in the wavelength range between 372 nm and 413 nm were determined at 2 mbar Ar pressure (distance 6 mm from the sample surface).

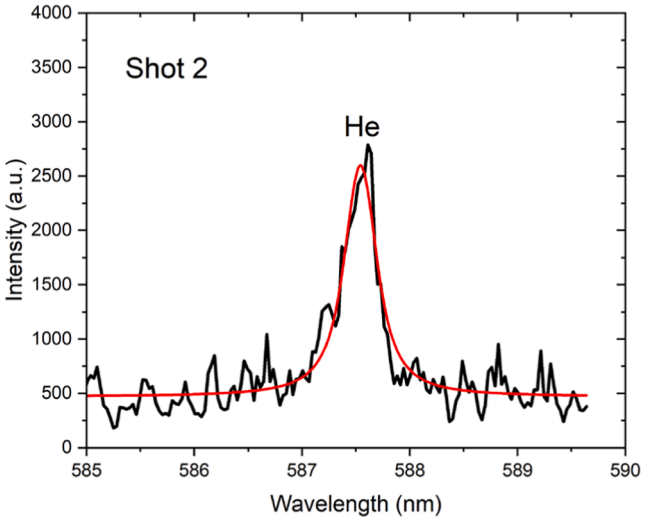

Fig. 4. Example of the spectrum for a He line at 587.56 nm (black line) collected during the 2nd LIBS shot at the same position with a delay time of 200 ns at 2 mbar Ar background pressure (distance 6 mm from the sample). Fitting with a Voigt profile is shown as a red line. (For interpretation of the references to colour in this figure legend, the reader is referred to the web version of this article.)

3.3. Construction of elemental depth profile

The elemental depth profiles shown in Fig. 5 were constructed from the intensities of Be I 381.34 nm line, W I 400.89 nm line, D 656.10 nm line and He 587.56 nm line at the distance of 6 mm and pressure 2 mbar. The intensity of the Be 381.34 nm line started to decrease after the 16th laser shot, coinciding with the emergence of the W line and the plateau for the W line was reached at about the 20th laser shot. The number of pulses required to reach half of the plateau value (18 shots in Fig. 5) was used to denote the interface between the coating and the substrate. It can be expected that this interface was actually ablated gradually due to the roughness of the substrate and the Gaussian shape of the laser beam resulting in the uneven ablation of the material. This also explains the gradual change of the line intensities after the 16th laser shot. When using the thickness of the coating between 4500–5000 nm and the approximate number of 18 laser shots required to ablate through the coating, the average ablation rate was 250–280 nm/shot. This ablation rate is comparable to the rates that were determined for other Be-containing coatings [17,18,20].

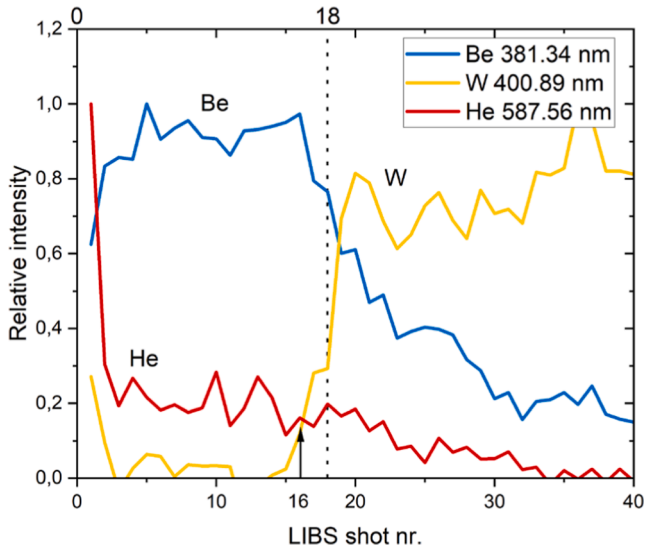

Fig. 5. Normalized LIBS depth profiles for Be, W and He lines (distance 6 mm from the sample). The arrow shows the laser shot number where the W lines started to appear and the dashed line shows the laser shot number where the W line intensity reached half of the plateau value corresponding to the bulk of the W substrate.

The intensity of the He line was higher during the first laser shot and then decreased to a lower level. This nearly constant level was kept up to 20–21 laser shots with only a slight decrease in He line intensity. At higher shot numbers, the intensity decreased to noise level which was reached after approximately 35 laser shots. The increased He signal during the first laser shot is not consistent with ToF-ERDA measurements, where He signal remained the same. Therefore, the increased He line intensity during the first laser shot is either due to the laser-induced outgassing of He or due to the different laser plasma plume properties caused by different properties of the surface layer of the coating. The outgassing can be an important factor for the reduced LIBS D intensity after the first laser shot as shown by a recent study [35]. However, the importance of outgassing of He remains less clear. The material surfaces have different mechanical and chemical properties from the bulk and, therefore, are expected to result in different ablation and different plasma plume properties. This matrix effect can also result in increased He line intensity during the first laser shot. A similar matrix effect is expected at the interface between the coating and the substrate.

The relatively constant value of He line intensity from shots 2–21 corresponding to the LIBS signal from the Be coating allowed the averaging of the spectra over the 20 successive laser shots, that is averaging each point in the spectrum over multiple shots (such as the spectrum corresponding to shot 2 shown in Fig. 4) to construct a new averaged spectrum with lower noise level. We checked that the values for the intensity and FWHM of the He 587.56 nm line of this average spectrum resulted in the same values as the average intensity and FWHM of the individual spectra recorded from the contributing 20 pulses.

The limit of detection (LOD) for the He 587.56 nm line intensity with the applied LIBS parameters was determined from the standard deviation of the background intensity s_B: LOD = $3s_B \cdot c_{He}/I_{He}$ [36], where c_{He} = 2.8 at. % and I_{He} = 740 (a.u.) is the average He line intensity from shots 2–21. The spectral range which was used for the calculation of s_B was the same as the range used to determine the intensity of the He line (587.25–587.85 nm) but the spectra corresponded to the laser shots 81–100 where the signal originated from the W substrate where He was missing. The average value of the standard deviation over shots 81–100 was s_B = 62. As a result, the LOD = 0.7 at. % was obtained. This detection limit is consistent with the results of our previous study where He could not be detected by the LIBS method in Be coatings with 0.54 % He by LIBS [21].

3.4. He line intensity at different distances in the plasma plume

The averaged spectra described in the previous paragraph were determined at different positions along the plasma plume and are shown in Fig. 6. Averaging was required because the spectra registered at other distances resulted in considerably weaker He signal and the He 587.56 nm lines of single spectra collected at the distance of 11 mm were at the noise level.

The intensity of the He 587.56 nm line was the strongest at a distance of 6 mm from the target. Closer to the target, at 3 mm, the intensity was smaller and farther from the target, at 11 mm, the intensity dropped to almost zero. Similar dependence on distance was determined for the Be 381.34 nm line (Fig. 7a). The width of the He line also depended on the distance and was peaking at a distance of 6 mm (Fig. 7b). This suggests that the plasma density was the highest at this distance.

3.5. He line intensity at different pressures

The averaged spectra of the He 587.56 nm line collected at increasing pressures are shown in Fig. 8. With increasing Ar pressure, the He line broadened and its maximum shifted towards shorter wavelengths. In addition, the intensity of the background emission increased and resulted in a larger noise of the signal. The lines collected at different pressures were fitted by Voigt profiles.

The intensity of the He 587.56 nm line increased with pressure and started to reach a plateau at 20 mbar (Fig. 9a). At the same time, the line width increased almost linearly with pressure and there was a noticeable shift of the position of the peak maximum towards smaller wavelengths. Both effects are caused by the increase of electron densities which occurs at higher pressures. The FWHM value of the He line was used to calculate the electron density [37] which increased from 1×10^{17} cm^{-3} to 1.3×10^{18} cm^{-3} when the pressure increased from 4 to 40 mbar. Similar electron density values were obtained from the shift of the central wavelength of the He 587.56 nm line when assuming the electron temperature of 1.7–1.8 eV. This temperature is consistent with the temperature assessed by the Boltzmann plot method (section 3.6).

Increasing pressure results in the reduction of the dimensions of the plasma plume [38,39], and the ablated material will be concentrated into a smaller volume. This increases the electron density and electron temperature [22,38,39] which can explain the increasing He line intensity. Another factor to consider is that the smaller the plume the more

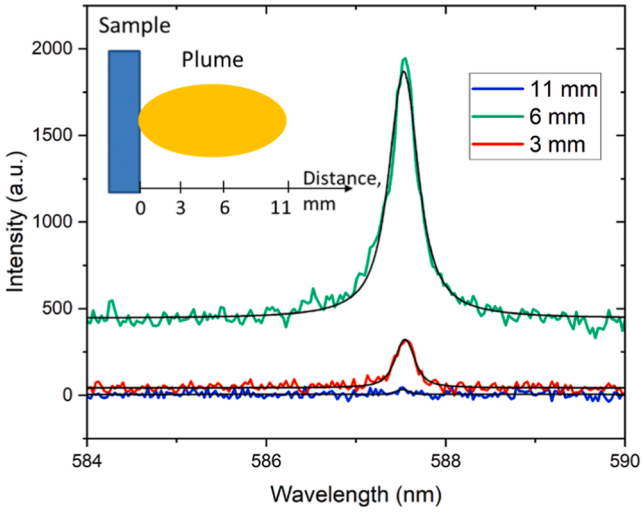

Fig. 6. Averaged LIBS spectra around the He 587.56 nm line were determined at three positions along the plasma plume at 2 mbar Ar pressure and a delay time of 200 ns. The schematic plume image with the corresponding distance values is shown in the inset. Black lines show the fitting results by Voigt profiles.

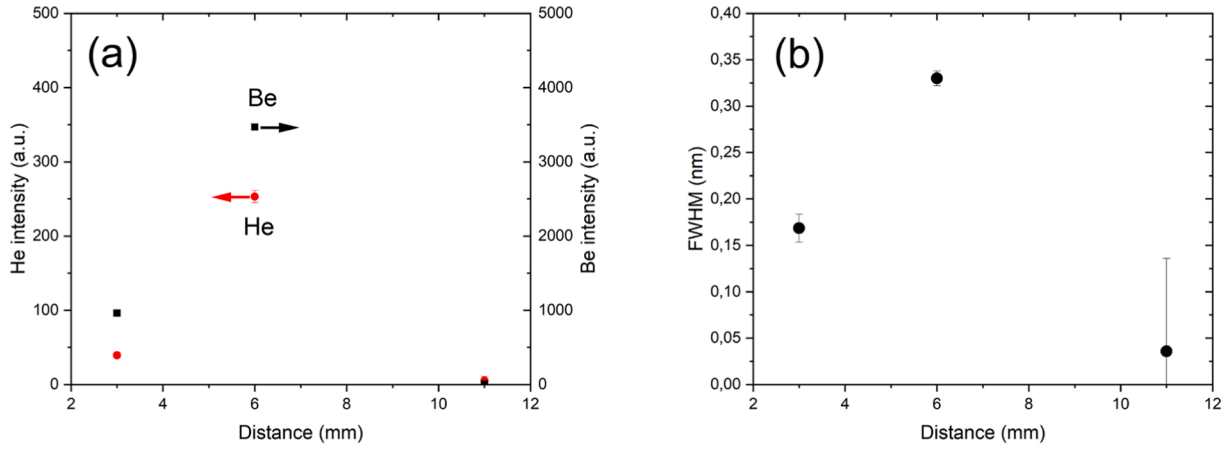

Fig. 7. (a) intensities of the He 587.56 nm and Be 381.34 nm lines and (b) width of the Lorentz component of the Voigt profile used to fit the He 587.56 nm line as a function of distance from the target surface at 2 mbar Ar pressure. The arrows point to the axis showing the He and Be intensities respectively.

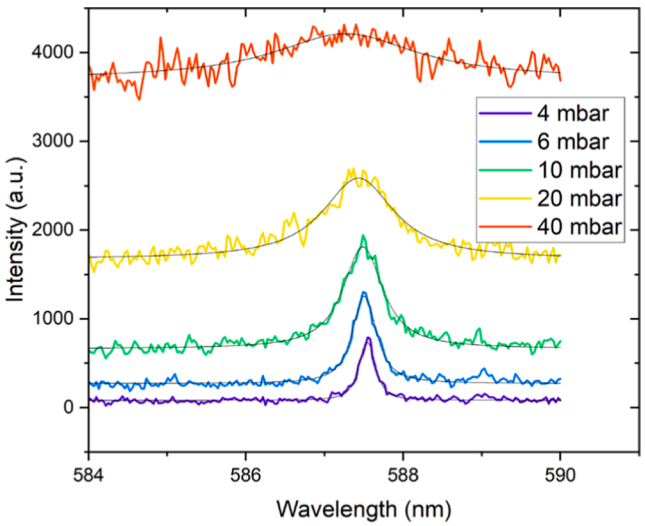

Fig. 8. Averaged LIBS spectra around the He 587.56 nm line were determined at variable Ar pressures (distance 3 mm). Black lines show the fitting results by Voigt profiles.

of the total emission is recorded by the optical fiber. It should be noted that these measurements were carried out at a closer distance to the target (3 mm) to account for smaller plume dimensions at higher pressures. The plume region where the intensity achieves its maximum also shifts closer to the target at higher pressures [38,40], potentially explaining the apparent increase in the line intensity and electron density in this regime.

The results demonstrate that at higher pressures, the determination of the He line intensity becomes limited by strong Stark broadening and increased noise. The electron density and Stark broadening reduce with longer delay times but the intensity of the relevant He line will also decrease. Further studies are required to investigate the influence of the increasing plasma pressures on the He line intensity at different distances in the plasma plume and increasing delay times.

3.6. *Applicability of calibration-free LIBS*

One possibility to determine the quantitative He content by LIBS is by the application of the calibration-free LIBS (CF-LIBS) method [41,42]. CF-LIBS gives reliable results when certain conditions of the plasma plume are fulfilled: (1) stoichiometric ablation to ensure that the plasma composition is representative of the target composition; (2) plasma is in Local Thermodynamic Equilibrium (LTE) in the temporal and spatial observation window; (3) the plasma is a spatially homogeneous source; (4) the spectral lines used in the calculation are optically thin. The registered intensities of the spectral lines I_{ki}^{λ} are related to the population of the excited level $N_k = N_s g_k \exp(-E_k/k_B T)/U^s(T)$ of the specimen s according to formula:

$$I_{ki}^{\lambda} = F N_k A_{ki} = F N_s g_k A_{ki}/\lambda_{ki} \exp(-E_k/k_B T)/U^s(T) \quad (1)$$

where F accounts for the fraction of photons recorded by the detection system, N_s is the total number density of species s in the plasma, λ_{ki} is the wavelength of the line, A_{ki} is the transition probability for transitions from excited level k to a lower level i, g_k is the statistical weight and E_k the excitation energy of the excited level k, k_B the Boltzmann constant, T the temperature in K, and $U^s(T)$ is the internal partition function of

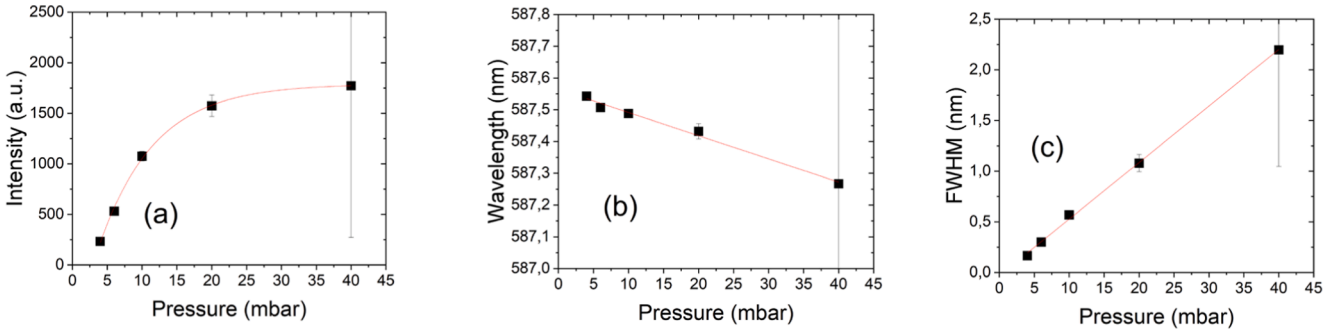

Fig. 9. (a) Intensity of the He 587.56 nm line, (b) wavelength of the line maximum and (c) FWHM value of Lorentzian profile of the He 587.56 nm line as a function of the Ar pressure.

species s at temperature T. The equation can be rewritten as:

$$\ln\left(I^{\lambda}_{ki}\lambda_{ki}/g_kA_{ki}\right) = -E_k/k_BT + \ln(FN_s/U^s(T)) \quad (2)$$

The values of $\ln\left(I^{\lambda}_{ki}\lambda_{ki}/g_kA_{ki}\right)$ corresponding to different lines of the same element at a certain ionized state can be plotted as a function of E_k in the Boltzmann plots. In the case of LTE, the dependence is linear with the slope of the linear fitting, giving the temperature of the LIBS plasma while the intercept is related to the concentration of species. When the Boltzmann plots are available for each element, it is possible to calculate their relative concentration in the studied sample. When the lines of certain elements are missing, the ratios of the identified species can be calculated from the intercepts of Boltzmann plots or, alternatively, from the ratios of single line intensities of the respective species according to Eq. (1) by using the temperature determined from the Boltzmann plot.

In the present study, there were only a few clearly detectable Be lines and the construction of the Boltzmann plot from Be lines was not feasible. Therefore, the intensities of Ar II lines in the wavelength range of 415–455 nm (namely 422.82 nm, 426.65 nm, 427.75 nm, 440.10 nm, 448.18 nm and 454.51 nm) were used to construct the Boltzmann plot. For improved signal strength, the intensities were further averaged over the shots of 2–21 where the Ar intensity remained nearly the same. The temperature determined from the Boltzmann plot of these Ar II lines was approximately 1.7 ± 0.2 eV (Fig. 10). This temperature also complies with the temperature evaluated from the shift of the He 587.56 nm line as described in sub-chapter 3.3. Similar temperatures obtained from the Boltzmann plot of Ar II lines were also observed in our previous paper [21] at similar experimental conditions and for a similar sample of BeD10Ne5.

The temperature determined from Ar II lines was used to calculate the He/Be concentration ratio from the ratio of He 587.56 nm and Be II 467.33 nm line intensities. The intensity ratio was 0.035 and the corresponding ratio of He neutrals and Be ions was 1.8. The ratio of ions and neutrals can be calculated by the Saha equation,

$$\frac{n_e n_s^{II}}{n_s^{I}} = \frac{(2\pi m_e k_B T)^{3/2}}{h^3}\frac{2U_s^{II}(T)}{U_s^{I}(T)}e^{-E_i/k_BT}, \quad (3)$$

where n_e and m_e are electron density and mass, h is Planck constant and other variables have been defined previously. The calculated ratio of the Be ion and neutral number densities n_s^{II} and n_s^{I} was approximately 300 when using an electron density 10^{17} cm^{-3} determined from the FWHM value of He 587.56 nm line. This means that practically all Be was in an ionized state. However, a considerable amount of Be atoms are already doubly ionized with the ratio of approximately 2. Therefore, it could be assumed that Be II ion concentration is about one third of the total Be concentration. The estimated He/Be ratio of 0.6 was more than an order of magnitude higher than the ratio determined by ToF-ERDA.

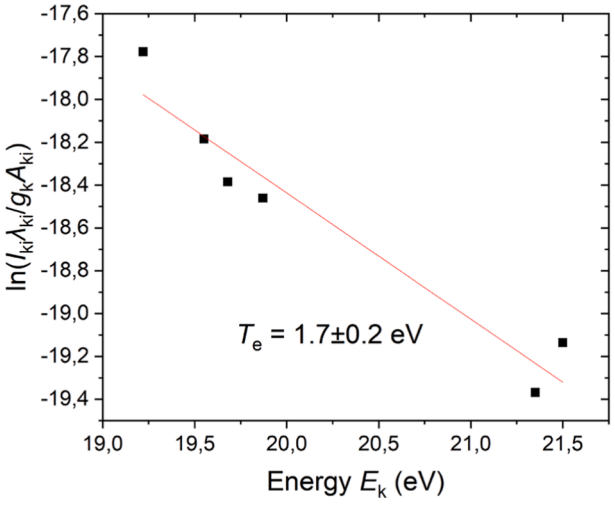

Fig. 10. Boltzmann plot with Ar II lines in the wavelength range of 415–455 nm. The line intensities were determined at 2 mbar (at 6 mm distance from the sample). The used intensities were average of laser shots 2–21.

The large discrepancy suggests that the conditions for CF-LIBS were not fulfilled. The McWhirter criterium for the electron density is expressed as $n_e \geq 1.6 \times 10^{12} T^{1/2}(\Delta E)^3$ where the electron density is in the units of cm^{-3}, T is the temperature in the units of K and E is largest energy difference between the excited levels, usually in ground state and lowest lying excited state, in the units of eV. The excitation energy of the lowest lying He metastable level is 19.8 eV and the electron densities required to fulfill the McWhirter criterion are approximately 1.7×10^{18} cm^{-3} [43]. The experimentally determined electron density 10^{17} cm^{-3} at 2 mbar Ar pressure is an order of magnitude lower and therefore the LTE could not be achieved in the laser generated plasma plume containing He. The McWhirter criterion could be fulfilled at higher pressures as shown in chapter 3.5 but at these conditions, the determination of the line intensity becomes very complicated due to the large broadening of the He line.

As a comparison, the McWhirther criterion for hydrogen isotopes is fulfilled at electron densities above 2×10^{17} cm^{-3} for our estimated electron temperature T_e and therefore the McWhirther criterion is more easily met for hydrogen isotopes. The fulfillment of another LTE condition, that the relaxation time should be faster than the decay time, is also more complicated to achieve in the case of He [43]. This is one possible explanation why the CF-LIBS method has been successfully applied for D concentration measurement in Be containing coatings [19,20] but appears to be less successful for He concentration measurement.

4. Conclusions

The present study investigated the usability of the LIBS method for the detection of He impurities retained in Be coatings simulating the co-deposits on the divertor plasma facing components of JET. According to the results of current measurements, 2.8 at. % of He in the Be coating is distinctly detectable at suitable LIBS conditions. The detection limit of He in such deposits should be approximately an order of magnitude smaller and therefore below 0.7 at. %.

He determination was successful only at lower pressures. The He line intensity increased at increasing pressures, but the simultaneous increase of electron density in the plasma plume caused considerable broadening of the He line and an increase of the background intensity and noise around the He line. As a result, at 40 mbar Ar pressure, the broad He line was barely distinguishable from the background. The effect of broadening caused at higher pressures becomes more severe in the case of He when compared to hydrogen isotopes. Higher excitation energy of He levels requires higher plasma temperatures and plasma densities to obtain sufficiently strong He lines and the broadening of the He line is therefore more important. Furthermore, the broadening of He lines is linearly dependent on the electron density while the broadening of hydrogen lines is a sublinear function. The electron densities depend on the spatial position in the plasma plume and on the delay times and it is necessary to conduct more studies to find the optimal conditions for the detection of Helium at higher pressures.

The application of the CF-LIBS procedure to the experimental data measured at low pressure conditions resulted in the overestimation of the He/Be ratio by more than an order of magnitude. In the case of He, the LTE conditions required for the application of CF-LIBS are harder to achieve when compared to hydrogen isotopes. However, the deviation from LTE is favorable for He detection because the signal would be too weak at low He concentrations when LTE conditions are met. The quantitative determination of He concentration by CF-LIBS requires more studies at different gas atmosphere pressures to further optimize the spatio-temporal window of LIBS plasma-plume development where

the LTE conditions can be met.

CRediT authorship contribution statement

Indrek Jõgi: Writing – review & editing, Writing – original draft, Formal analysis. **Peeter Paris:** Writing – review & editing, Methodology, Investigation. **Jasper Ristkok:** Writing – review & editing, Investigation. **Alicia Marin Roldán:** Writing – review & editing, Investigation, Data curation. **Pavitra Ganapati Bhat:** Writing – review & editing, Validation, Formal analysis. **Pavel Veis:** Writing – review & editing, Validation. **Juuso Karhunen:** Writing – review & editing, Methodology, Investigation. **Salvatore Almaviva:** Writing – review & editing, Investigation. **Wojciech Gromelski:** Writing – review & editing, Investigation, Data curation. **Paul Dinca:** Writing – review & editing, Resources. **Corneliu Porosnicu:** Writing – review & editing, Resources. **Iva Bogdanović Radović:** Writing – review & editing, Investigation. **Zdravko Siketić:** Writing – review & editing, Investigation. **Paweł Gąsior:** Writing – review & editing. **Jari Likonen:** Writing – review & editing, Supervision, Resources, Investigation. **Antti Hakola:** Writing – review & editing, Supervision, Project administration, Methodology, Investigation.

Declaration of competing interest

The authors declare that they have no known competing financial interests or personal relationships that could have appeared to influence the work reported in this paper.

Data availability

Data will be made available on request.

Acknowledgements

This work has been carried out within the framework of the EUROfusion Consortium, funded by the European Union via the Euratom Research and Training Programme (Grant Agreement No 101052200—EUROfusion). Views and opinions expressed are however those of the author(s) only and do not necessarily reflect those of the European Union or the European Commission. Neither the European Union nor the European Commission can be held responsible for them.

The authors from Comenius University acknowledge partial financial support from Agencies under the project numbers (VEGA-1/0803/21 and APVV-22-0548). This scientific paper has been published as part of the international project co-financed by the Polish Ministry of Science and Higher Education within the programme called 'PMW' for 2023-2024.

References

[1] G.F. Matthews, P. Edwards, T. Hirai, M. Kear, A. Lioure, P. Lomas, A. Loving, C. Lungu, H. Maier, P. Mertens, D. Neilson, R. Neu, J. Pamela, V. Philipps, G. Piazza, V. Riccardo, M. Rubel, C. Ruset, E. Villedieu, M. Way, Overview of the ITER-like wall project, Phys. Scr. T128 (2007) 137–143, https://doi.org/10.1088/0031-8949/2007/T128/027.

[2] G.F. Matthews, M. Beurskens, S. Brezinsek, M. Groth, E. Joffrin, A. Loving, M. Kear, M.L. Mayoral, R. Neu, P. Prior, V. Riccardo, F. Rimini, M. Rubel, G. Sips, E. Villedieu, P. De Vries, M.L. Watkins, JET ITER-like wall - Overview and experimental programme, Phys. Scr. t T145 (2011) 014001, https://doi.org/10.1088/0031-8949/2011/T145/014001.

[3] S. Brezinsek, W. Fundamenski, TEich, J.P. Coad, C. Giroud, A. Huber, S. Jachmich, E. Joffrin, K. Krieger, K. McCormick, M. Lehnen, T. Loarer, E. De La Luna, G. Maddison, G.F. Matthews, P. Mertens, I. Nunes, V. Philipps, V. Riccardo, M. Rubel, M.F. Stamp, M. Tsalas, Overview of experimental preparation for the ITER-Like Wall at JET, J. Nucl. Mater. 415 (2011) S936–S942, https://doi.org/10.1016/j.jnucmat.2010.10.037.

[4] R.A. Pitts, S. Carpentier, F. Escourbiac, T. Hirai, V. Komarov, A.S. Kukushkin, S. Lisgo, A. Loarte, M. Merola, R. Mitteau, A.R. Raffray, M. Shimada, P.C. Stangeby, Physics basis and design of the ITER plasma-facing components, J. Nucl. Mater. 415 (2011) S957–S964, https://doi.org/10.1016/j.jnucmat.2011.01.114.

[5] G. De Temmerman, M.J. Baldwin, D. Anthoine, K. Heinola, A. Jan, I. Jepu, J. Likonen, C.P. Lungu, C. Porosnicu, R.A. Pitts, Efficiency of thermal outgassing for tritium retention measurement and removal in ITER, Nucl. Mater. Energy. 12 (2017) 267–272, https://doi.org/10.1016/j.nme.2016.10.016.

[6] J. Roth, E. Tsitrone, T. Loarer, V. Philipps, S. Brezinsek, A. Loarte, G.F. Counsell, R. P. Doerner, K. Schmid, O.V. Ogorodnikova, R.A. Causey, Tritium inventory in ITER plasma-facing materials and tritium removal procedures, Plasma Phys. Control. Fusion. 50 (2008) 103001, https://doi.org/10.1088/0741-3335/50/10/103001.

[7] K. Heinola, A. Widdowson, J. Likonen, E. Alves, A. Baron-Wiechec, N. Barradas, S. Brezinsek, N. Catarino, P. Coad, S. Koivuranta, G.F. Matthews, M. Mayer, P. Petersson, Fuel retention in JET ITER-Like Wall from post-mortem analysis, J. Nucl. Mater. 463 (2015) 961–965, https://doi.org/10.1016/j.jnucmat.2014.12.098.

[8] K. Heinola, A. Widdowson, J. Likonen, E. Alves, A. Baron-Wiechec, N. Barradas, S. Brezinsek, N. Catarino, P. Coad, S. Koivuranta, S. Krat, G.F. Matthews, M. Mayer, P. Petersson, J.E.T. Contributors, Long-term fuel retention in JET ITER- like wall, Phys. Scr T167 (2016) 014075, https://doi.org/10.1088/0031-8949/T167/1/014075.

[9] G. De Temmerman, K. Heinola, D. Borodin, S. Brezinsek, R.P. Doerner, M. Rubel, E. Fortuna-Zaleśna, C. Linsmeier, D. Nishijima, K. Nordlund, M. Probst, J. Romazanov, E. Safi, T. Schwarz-Selinger, A. Widdowson, B.J. Braams, H. K. Chung, C. Hill, Data on erosion and hydrogen fuel retention in Beryllium plasma-facing materials, Nucl. Mater. Energy. 27 (2021) 100994, https://doi.org/10.1016/j.nme.2021.100994.

[10] D. Alegre, M.J. Baldwin, M. Simmonds, D. Nishijima, E.M. Hollmann, S. Brezinsek, R.P. Doerner, A parametric study of helium retention in beryllium and its effect on deuterium retention, Phys. Scr (2017) 014028, https://doi.org/10.1088/1402-4896/aa8c99.

[11] A. Založnik, M.J. Baldwin, R.P. Doerner, T. Schwarz-Selinger, S. Brezinsek, The influence of helium on deuterium retention in beryllium co-deposits, J. Nucl. Mater. 512 (2018) 25–30, https://doi.org/10.1016/j.jnucmat.2018.09.032.

[12] A. Malaquias, V. Philipps, A. Huber, A. Hakola, J. Likonen, J. Kolehmainen, S. Tervakangas, M. Aints, P. Paris, M. Laan, A. Lissovski, S. Almaviva, L. Caneve, F. Colao, G. Maddaluno, M. Kubkowska, P. Gasior, H.J. Van Der Meiden, A.R. Lof, P.A. Zeijlmans Van Emmichoven, P. Petersson, M. Rubel, E. Fortuna, Q. Xiao, Development of ITER relevant laser techniques for deposited layer characterisation and tritium inventory, J. Nucl. Mater. 438 (2013) S936–S939, https://doi.org/10.1016/j.jnucmat.2013.01.203.

[13] H.J. Van Der Meiden, S. Almaviva, J. Butikova, V. Dwivedi, P. Gasior, W. Gromelski, A. Hakola, X. Jiang, I. Jõgi, J. Karhunen, M. Kubkowska, M. Laan, G. Maddaluno, A. Marín-Roldán, P. Paris, K. Piip, M. Pisarčík, G. Sergienko, M. Veis, P. Veis, S. Brezinsek, Monitoring of tritium and impurities in the first wall of fusion devices using a LIBS based diagnostic, Nucl. Fusion. 61 (2021) 125001, https://doi.org/10.1088/1741-4326/ac31d6.

[14] M. Imran, Z. Hu, F. Ding, M. Li, G.N. Luo, H. Sattar, M. Iqbal, H. Ding, Diagnostic study of impurity deposition in fusion device by calibration-free laser-induced breakdown spectroscopy, Spectrochim. Acta - Part B at. Spectrosc. 198 (2022) 106568 https://doi.org/10.1016/j.sab.2022.106568.

[15] D. Zhao, C. Li, Z. Hu, C. Feng, Q. Xiao, R. Hai, P. Liu, L. Sun, D. Wu, C. Fu, J. Liu, N. Farid, F. Ding, G.N. Luo, L. Wang, H. Ding, Remote in situ laser-induced breakdown spectroscopic approach for diagnosis of the plasma facing components on experimental advanced superconducting tokamak, Rev. Sci. Instrum. 89 (2018) 073501, https://doi.org/10.1063/1.5024848.

[16] C. Li, L. Sun, Z. Hu, D. Zhao, J. Liu, N. Gierse, D. Nicolai, D. Wu, R. Hai, F. Ding, G. N. Luo, S. Brezinsek, C. Linsmeier, Y. Liang, H. Ding, An in situ diagnostic method for monitoring of fuel retention on the first wall under long-pulse operation of experimental advanced superconducting tokamak, Phys. Scr 014069 (2020), https://doi.org/10.1088/1402-4896/ab6005.

[17] M. Suchonova, P. Veis, J. Karhunen, P. Paris, M. Pribula, K. Piip, M. Laan, C. Porosnicu, C. Lungu, A. Hakola, Determination of deuterium depth profiles in fusion-relevant wall materials by nanosecond LIBS, Nucl. Mater. Energy. 12 (2017) 611–616, https://doi.org/10.1016/j.nme.2017.05.013.

[18] J. Karhunen, A. Hakola, J. Likonen, A. Lissovski, M. Laan, P. Paris, Applicability of LIBS for in situ monitoring of deposition and retention on the ITER-like wall of JET - Comparison to SIMS, J. Nucl. Mater. 463 (2015) 931–935, https://doi.org/10.1016/j.jnucmat.2014.10.028.

[19] P. Veis, A. Marin-Roldan, V. Dwivedi, J. Karhunen, P. Paris, I. Jõgi, C. Porosnicu, C. P. Lungu, V. Nemanic, A. Hakola, Quantification of H/D content in Be/W mixtures coatings by CF-LIBS, Phys. Scr. T171 (2020) 014073, https://doi.org/10.1088/1402-4896/ab7ebd.

[20] V. Dwivedi, A. Marín-Roldán, J. Karhunen, P. Paris, I. Jõgi, C. Porosnicu, C. P. Lungu, H. van der Meiden, A. Hakola, P. Veis, CF-LIBS quantification and depth profile analysis of Be coating mixed layers, Nucl. Mater. Energy. 27 (2021) 100990, https://doi.org/10.1016/j.nme.2021.100990.

[21] P.G. Bhat, P. Veis, A.M. Roldán, J. Karhunen, P. Paris, I. Jõgi, A. Hakola, LIBS depth profiling of Be-containing samples with different gaseous impurity concentrations, Nucl. Mater. Energy. 37 (2023) 101549, https://doi.org/10.1016/j.nme.2023.101549.

[22] D. Nishijima, E.M. Hollmann, R.P. Doerner, D.L. Rudakov, Laser-induced breakdown spectroscopy analyses of tungsten surfaces, Phys. Scr. (2016) 014032, https://doi.org/10.1088/0031-8949/T167/1/014032.

[23] K. Piip, H.J. van der Meiden, K. Bystrov, L. Hämarik, J. Karhunen, M. Aints, M. Laan, P. Paris, H. Seemen, A. Hakola, S. Brezinsek, Loading of deuterium and helium by Pilot-PSI plasma and their detection by in-situ LIBS, Nucl. Mater. Energy. 12 (2017) 694–698, https://doi.org/10.1016/j.nme.2016.12.034.

[24] G. Shaw, M. Bannister, T.M. Biewer, M.Z. Martin, F. Meyer, B.D. Wirth, The detection of He in tungsten following ion implantation by laser-induced breakdown spectroscopy, Appl. Surf. Sci. 427 (2018) 695–703, https://doi.org/10.1016/j.apsusc.2017.08.180.
[25] G. Shaw, W. Garcia, X. Hu, B.D. Wirth, Investigating helium-deuterium synergies in plasma-exposed tungsten using laser ablation techniques, Phys. Scr. 2020 (2020) 014029, https://doi.org/10.1088/1402-4896/ab47c7.
[26] Z. He, Y. Lyu, D. Wu, R. Hai, X. Bai, H. Wu, H. Ding, Quantitative characterization of helium in the ITER-like co-deposition layer by laser-induced breakdown spectroscopy, Nucl. Mater. Energy. 36 (2023) 101493, https://doi.org/10.1016/j.nme.2023.101493.
[27] P. Dinca, C. Staicu, C. Porosnicu, O.G. Pompilian, A.M. Banici, B. Butoi, C.P. Lungu, I. Burducea, Deuterium retention and release behavior from beryllium co-deposited layers at distinct Ar/D ratio, Coatings. 11 (2021) 1–13, https://doi.org/10.3390/coatings11121443.
[28] P. Dinca, C. Staicu, C. Porosnicu, B. Butoi, O.G. Pompilian, A.M. Banici, F. Baiasu, I. Burducea, C.P. Lungu, Deuterium retention in mixed layers with application in fusion technology, Coatings. 12 (2022) 951, https://doi.org/10.3390/coatings12070951.
[29] P. Dinca, C. Porosnicu, B. Butoi, I. Jepu, V. Tiron, O.G. Pompilian, I. Burducea, C. P. Lungu, I.L. Velicu, Beryllium-tungsten study on mixed layers obtained by m-HiPIMS/DCMS techniques in a deuterium and nitrogen reactive gas mixture, Surf. Coatings Technol. 321 (2017) 397–402, https://doi.org/10.1016/j.surfcoat.2017.04.074.
[30] Z. Siketić, I.B. Radović, M. Jakšić, Development of a time-of-flight spectrometer at the Ruder Bošković Institute in Zagreb, Nucl. Instruments Methods Phys. Res. Sect. B Beam Interact. with Mater. Atoms. 266 (2008) 1328–1332, https://doi.org/10.1016/j.nimb.2007.12.070.
[31] Z. Siketić, I.B. Radović, M. Jakšić, N. Skukan, Time of flight elastic recoil detection analysis with a position sensitive detector, Rev. Sci. Instrum. 81 (2010) 033305, https://doi.org/10.1063/1.3356976.
[32] K. Arstila, J. Julin, M.I. Laitinen, J. Aalto, T. Konu, S. Kärkkäinen, S. Rahkonen, M. Raunio, J. Itkonen, J.P. Santanen, T. Tuovinen, T. Sajavaara, Potku - New analysis software for heavy ion elastic recoil detection analysis, Nucl. Instruments Methods Phys. Res. Sect. B Beam Interact. with Mater. Atoms. 331 (2014) 34–41, https://doi.org/10.1016/j.nimb.2014.02.016.
[33] A. Hakola, J. Likonen, L. Aho-Mantila, M. Groth, S. Koivuranta, K. Krieger, T. Kurki-Suonio, T. Makkonen, M. Mayer, H.W. Müller, R. Neu, V. Rohde, Migration and deposition of 13C in the full-tungsten ASDEX Upgrade tokamak, Plasma Phys. Control. Fusion 52 (2010) 065006, https://doi.org/10.1088/0741-3335/52/6/065006.
[34] T. Ida, M. Ando, H. Toraya, Extended pseudo-Voigt function for approximating the Voigt profile, J. Appl. Crystallogr. 33 (2000) 1311–1316, https://doi.org/10.1107/S0021889800010219.
[35] D. Matveev, X. Jiang, G. Sergienko, A. Kreter, S. Brezinsek, C. Linsmeier, Short-term retention in metallic PFCs: Modelling in view of mass spectrometry and LIBS, Phys. Scr 96 (2021) 124079, https://doi.org/10.1088/1402-4896/ac43d6.
[36] G.L. Long, J.D. Winefordner, Limit of Detection. A Closer Look at the IUPAC Definition, Anal. Chem. 55 (1983) 712–724, https://doi.org/10.1021/ac00258a724.
[37] G.L. Long, J.D. Winefordner, Limit of Detection, A Closer Look at the IUPAC Definition, Report, Anal. Chem 55 (1983) 712–724, https://doi.org/10.1021/ac00258a724.
[38] J.A. Aguilera, C. Aragón, Temperature and electron density distributions of laser-induced plasmas generated with an iron sample at different ambient gas pressures, Appl. Surf. Sci. 197–198 (2002) 273–280, https://doi.org/10.1016/S0169-4332(02)00382-3.
[39] S.B. Wen, X. Mao, R. Greif, R.E. Russo, Laser ablation induced vapor plume expansion into a background gas. II. Experimental analysis, J. Appl. Phys. 101 (2007) 023115, https://doi.org/10.1063/1.2431085.
[40] S.S. Harilal, C.V. Bindhu, M.S. Tillack, F. Najmabadi, A.C. Gaeris, Internal structure and expansion dynamics of laser ablation plumes into ambient gases, J. Appl. Phys. 93 (2003) 2380–2388, https://doi.org/10.1063/1.1544070.
[41] A. Ciucci, V. Palleschi, S. Rastelli, A. Salvetti, D.P. Singh, E. Tognoni, CF-LIPS: a new approach to LIPS spectra analysis, Laser Part. Beams. 17 (1999) 793–797, https://doi.org/10.1017/s0263034699174251.
[42] E. Tognoni, G. Cristoforetti, S. Legnaioli, V. Palleschi, Calibration-free laser-induced breakdown spectroscopy: state of the art, spectrochim, Acta - Part B at. Spectrosc. 65 (2010) 1–14, https://doi.org/10.1016/j.sab.2009.11.006.
[43] G. Cristoforetti, A. De Giacomo, M. Dell'Aglio, S. Legnaioli, E. Tognoni, V. Palleschi, N. Omenetto, Local thermodynamic equilibrium in laser-induced breakdown spectroscopy: beyond the mcwhirter criterion, spectrochim, Acta - Part B at. Spectrosc. 65 (2010) 86–95, https://doi.org/10.1016/j.sab.2009.11.005.